LBL-36050
UC-410

Lawrence Berkeley Laboratory
UNIVERSITY OF CALIFORNIA

Materials Sciences Division

Presented at the Fourth IKETANI Conference on "Optically Nonlinear Organic Materials and Applications," Kamuela, Hawaii, May 16–18, 1994 and to be published in the Proceedings

Nonlinear Optics and Organic Materials

Y.R. Shen

July 1994

Prepared for the U.S. Department of Energy under Contract Number DE-AC03-76SF00098

DISCLAIMER

LBL-36050
UC-410

Nonlinear Optics and Organic Materials

Y.R. Shen

Department of Physics
University of California

and

Materials Sciences Division
Lawrence Berkeley Laboratory
University of California
Berkeley, California 94720

July 1994

This work was supported by the Director, Office of Energy Research, Office of Basic Energy Sciences, Materials Science Division, of the U.S. Department of Energy under Contract No. DE-AC03-76SF00098, and by the National Science Foundation under Grant DMR-9025106.

LBL-36050
UC-410

NONLINEAR OPTICS AND ORGANIC MATERIALS

Y. R. SHEN

Department of Physics, University of California, and
Materials Science Division, Lawrence Berkeley Laboratory
Berkeley, California 94720

In recent years, we have witnessed a growing relationship between the organics and optics communities. Liquid crystals, for example, have become the preferred materials for optical display devices. Organics are being seriously considered as the materials of the future for optoelectronic applications. It is known that organic molecules with extensively delocalized electrons are highly nonlinear and could be used in the design of new nonlinear optical materials. Indeed, organic crystals and poled polymers with exceptionally strong second-order nonlinearities and good optical quality have been discovered. Numerous organic materials with high third-order nonlinearities have also been found. The recent discovery of organic photo-refractive materials has stimulated even more interest in this area. Many conferences have been devoted to this topic in the past ten years. The recent IKETANI Conference again had it as the main theme. Advances in the field have been exciting and encouraging, but I will refrain from further discussion and simply refer the readers to the many papers in this Special Issue. Instead, we shall consider another interesting topic relating nonlinear optics and organic materials: how nonlinear optics can be used to study organic materials.

One of the main differences between linear and nonlinear responses of a medium to incoming radiation is in their symmetries.[1] It leads to the possibility that some properties of the medium could be more sensitively probed by nonlinear, rather than linear, optical means, or vise versa. A well-known example is that some vibrational modes of a medium could be Raman-active but infrared-inactive, and would be more readily observed by Raman

scattering, which is a two-photon transition process. In this paper, we shall discuss, with the help of three examples, how we can use second harmonic generation (SHG) and sum frequency generation (SFG) to obtain unique information about a material. We shall focus on thin films, surfaces, and interfaces.

We discuss first the study of C_{60} films by SHG. The recently discovered fullerene materials are known to have fascinating physical properties.[2] Their hyperpolarizabilities are expected to be very large because of the extensive pi-electron delocalization on their cages. Accordingly, many studies of their optical nonlinearities have been reported in the literature.[3] However, by symmetry, the second-order nonlinearity of C_{60} is forbidden both microscopically and macroscopically. Magnetic dipole and electric quadrupole contributions to the second-order nonlinearity are allowed, and it turns out that SHG from C_{60} conveniently constitutes a test case for the theory of SHG from a centrosymmetric film. In addition, by tuning the optical frequency to magnetic dipole and electric quadrupole resonances, SHG provides a unique opportunity to probe the low-lying forbidden electronic transitions in C_{60}.

The nonlinear polarization of a medium can be written in the multipole expansion form: [1]

$$\mathbf{P}^{(2)}(2\omega) = \mathbf{P}_D^{(2)} - \nabla\cdot\overleftrightarrow{Q}^{(2)} + \frac{c}{i2\omega}\nabla\times\mathbf{M}^{(2)} + \ldots \qquad (1)$$

$$\mathbf{P}_D^{(2)} = \overleftrightarrow{\chi}_D^{(2)}:\mathbf{E}(\omega)\mathbf{E}(\omega) + \overleftrightarrow{\chi}_P^{(2)}:\mathbf{E}\nabla\mathbf{E}$$

$$\overleftrightarrow{Q}^{(2)} = \overleftrightarrow{\chi}_Q^{(2)}:\mathbf{E}\mathbf{E}.$$

For an isotropic bulk, which we shall assume for C_{60}, we have by symmetry the following:[4,5] $\mathbf{M} = 0$; $\overleftrightarrow{\chi}_D^{(2)} = 0$; $\overleftrightarrow{\chi}_p^{(2)}$ has 3 nonvanishing independent elements χ_{p2}, χ_{p3}, and χ_{p4}; $\overleftrightarrow{\chi}_Q^{(2)}$ has 2 nonvanishing independent elements χ_{Q2}, and χ_{Q3}. In the microscopic expressions, $\overleftrightarrow{\chi}_p^{(2)}$ involves an electric quadrupole or magnetic dipole transition

matrix element at the fundamental frequency in each term, and $\overleftrightarrow{\chi}^{(2)}_{Q}$ involves an electric quadrupole transition matrix element at the SH frequency in each term. Furthermore, we should have $\chi_{p3} = -\chi_{p4}$ if the magnetic dipole matrix element dominates in $\overleftrightarrow{\chi}^{(2)}_{p}$ and $\chi_{p3} = \chi_{p4}$ if the electric quadrupole matrix element dominates.

For SHG in transmission or reflection from a film sandwiched between air and an substrate, the signal can be expressed in the form[5]

$$S(2\omega) = \frac{32\pi^3\omega}{\hbar c^3 \epsilon^{1/2}(2\omega)\epsilon(\omega)} \sin^2\theta_{in} |\chi^{(2)}_{eff}|^2 I^2(\omega)\, AT \qquad (2)$$

where $\chi^{(2)}_{eff}$ is a function of film thickness, dielectric constants of the film and the surrounding media, angles of incidence and refraction, and the surface and bulk nonlinear susceptibilities of the film. For an isotropic film, there are three nonvanishing independent surface nonlinear susceptibility elements at the air/film interface, $\chi^{(2)}_{s,zzz}$, $\chi^{(2)}_{s,zyy}$, $\chi^{(2)}_{s,yzy}$, three similar ones at the film/quartz interface, $\chi^{(2)}_{I,zzz}$, $\chi^{(2)}_{I,zyy}$, $\chi^{(2)}_{I,yzy}$ and one bulk susceptibility element δ contributing to $\chi^{(2)}_{eff}$. They can be determined from the SHG measurements with different polarization combinations, rather accurately if SHG as a function of film thickness can be measured. By assuming that the surfaces of the film are simply a termination of the bulk structure with a continuous density variation, which should be a good approximation for C_{60} film, we can relate the early mentioned set of 5 bulk susceptibility elements χ_{2p}, χ_{3p}, χ_{4p}, χ_{Q2}, and χ_{Q3} to the present set of 7 elements $\chi^{(2)}_{s,zzz}$, $\chi^{(2)}_{s,zyy}$, $\chi^{(2)}_{s,yzy}$, $\chi^{(2)}_{I,zzz}$, $\chi^{(2)}_{I,zyy}$, $\chi^{(2)}_{I,yzy}$, and δ.

SHG experiments for C_{60} films on quartz substrates have actually been carried out in-situ during film growth in an ultrahigh vacuum chamber.[4,5] Figure 1 shows a typical set of data obtained from the same run with different polarization combinations in transmission

and reflection.[5] The experiment was performed at $\hbar\omega$ = 1.16 eV. A theoretical fit of the data allows the determination of the set of 7 parameters $\chi^{(2)}_{s,ijk}$, $\chi^{(2)}_{I,ijk}$, and δ and the set of 5 parameters χ_{pi} and χ_{Qi}. The results show that $|\chi_s| \sim |\chi_I| \sim \delta$ and $|\chi_p| \sim |\chi_Q|$ suggesting that for the C_{60} films the bulk and surface contributions to SHG are equally important and both electric dipole and electric quadrupole excitations at the fundamental frequency of 1.16 eV are significant. In a similar experiment using $\hbar\omega$ = 1.81 eV, Koopmans et al.[4] however found $|\chi_s| \sim |\chi_I| \ll \delta$ and $\chi_Q = 0$, $\chi_{p3} = -\chi_{p4}$, indicating that the magnetic dipole excitation at the fundamental frequency must have dominated. By scanning $\hbar\omega$ around 1.8 eV, they could indeed observe a resonance enhancement peaked at 1.81 eV. This magnetic dipole resonant transition is expected from the energy level diagram of C_{60},[6] but has never been observed by linear optical spectroscopy because it is too weak and sits on the tail of the allowed electric dipole absorption peak. In SHG, symmetry dictates the fact that the resonant enhancement near an electric dipole transition should be of the same order of magnitude as that near a magnetic dipole transition. This makes the magnetic dipole transition more easily detectable. The same argument applies to an electric quadrupole transition. Presumably by tuning $\hbar\omega$ around 2.2 eV, one could also find from resonant SHG the predicted electric quadrupole transition near the band gap in C_{60}. This is therefore a clear example of how SHG can provide unique information about the electronic properties of a material.

We now show SHG can also be used to study surface-induced bulk alignment of a liquid crystal cell. This is a problem of great importance in liquid crystal (LC) display technology.[6] The design of LC display devices relies critically on the bulk molecular alignment. It is believed that the orientation and alignment of single molecular monolayers at the surfaces of an LC film can effectively determine the bulk alignment.[7] For example, for LC display devices, homogeneous bulk alignment (LC molecules nearly parallel to

substrates) is often required. This is commonly achieved by rubbing polymer-coated substrates. Rubbing presumably stretches the surface polymer chains along a certain direction, which in turn aligns the first LC monolayer at the polymer surface.[8] Correlation between LC molecules then leads to the observed surface-induced bulk homogeneous alignment. To prove that this is the case, we need to measure the orientational distribution of the surface LC monolayer. The measurement can actually be done by SHG.[7] As a second-order nonlinear optical effect, it is forbidden in a medium with inversion symmetry but necessarily allowed at an interface. Therefore the process is highly surface-specific. Since it also has a submonolayer sensitivity, it becomes an ideal tool for surface studies. Here, we use it to measure the orientational distribution of an LC monolayer adsorbed on a rubbed polymer surface.

For a uni-directionally aligned LC monolayer, the corresponding nonlinear susceptibility tensor

$$\overleftrightarrow{\chi}^{(2)} = N \langle \overleftrightarrow{\alpha}^{(2)} \rangle \tag{3}$$

has 6 nonvanishing independent elements. Here, the angular brackets denote an orientational average, and for rod-like LC molecules such as 8CB (4'-n-octyl-4-cyanobiphenyl), the hyperpolarizability tensor is dominated by a single element $\alpha^{(2)}_{\zeta\zeta\zeta}$ along the long molecular axis. SHG from the LC monolayer as a function of azimuthal rotation should exhibit a two-fold symmetry. Figure 2 is an example. By fitting the experimental data with theory of SHG, we can deduce all the six independent elements of $\overleftrightarrow{\chi}^{(2)}$. Assuming that the monolayer orientational distribution takes the approximate form

$$f(\theta,\phi)\cdot\alpha \exp\left[- \frac{(\theta-\theta_0)^2}{2\sigma^2} \right] \left[1+d_1\cos\phi + d_2\cos 2\phi + d_3\cos 3\phi \right] \tag{4}$$

and using Eq. (3) with the deduced values of $\chi^{(2)}_{ijk}$, we can then find the parameters θ_0, σ, d_1, d_2 and d_3. From Fig. 2, for example, we obtain $\theta_0 = 78°$, $\sigma = 10°$, $d_1 = 0.13$, $d_2 = 0.69$, and $d_3 = 0.03$. The resulting azimuthal orientational distribution of the monolayer is plotted in Fig. 3.

The known orientational distribution permits the determination of the corresponding order parameter tensor of the surface LC monolayer defined by $\overleftrightarrow{Q} = \langle(3\zeta\zeta\text{-II})/2\rangle$. Using the Landau-de Gennes formalism, we can express the free energy of the LC film in terms of the spatially varying order parameter with $\overleftrightarrow{Q}(0)$ as the boundary condition. Minimization of the free energy then leads to the solution of $\overleftrightarrow{Q}(z)$, which in the limit of $z \rightarrow \infty$, completely specifies the bulk LC alignment including the so-called pretilt angle the molecules make with the substrate.[7] The pretilt angle is actually an important design parameter for LC displays, but so far how it can be affected by surface treatment is not understood. Using the above approach, we have successfully predicted the bulk 8 CB film alignments from the measured orientational distributions of 8 CB monolayers on polyimide-coated substrates rubbed with different strengths. (Stronger uni-directional rubbing yields a more anisotropic monolayer alignment and a larger pretilt angle.) The predictions agree remarkably well with the measured bulk alignment. The predicted pretilt angles are accurate to within 8%. This is a demonstration of how SHG can be used as a unique surface probe to help solve a scientific problem with important technological implication.

As a third example, we discuss the use of IR-visible SFG to obtain the first vibrational spectra of water interfaces and learn about the water interfacial structures.[9] This is a most exciting problem because water interfaces play a key role in many important physical, chemical, and biological systems and yet their structures are hardly known despite extensive theoretical and experimental effort in the past. Vibrational spectra are clearly important for the understanding of water interfaces, but they have never been observed by

conventional means. SFG is a second-order process and therefore is surface-specific. The output frequency ω is the sum of the input IR frequency ω_{IR} and the input visible frequency ω_{vis}. If ω_{IR} approaches a surface vibrational resonance, the SF output will experience a resonant enhancement. Thus the SFG spectrum obtained by scanning ω_{IR} over surface vibrational resonances should yield the surface vibrational spectrum. More specifically, SFG measures the nonlinear susceptibility tensor[9]

$$\overleftrightarrow{\chi}^{(2)} = \overleftrightarrow{\chi}_{NR}^{(2)} + \sum_{\alpha} \frac{\overleftrightarrow{A}_{\alpha}}{\omega_{IR}-\omega_{\alpha}+ i\Gamma_{\alpha}} \qquad (5)$$

which can be resonantly enhanced through the resonant denominator.

Figure 4 (A)--(C) exhibit a set of SFG spectra for various water interfaces.[9] Consider first the spectrum of Fig. 4(B) for the air/water interface. It apparently is composed of three peaks at roughly 3200, 3450, and 3700 cm^{-1}, respectively. The narrow peak at 3700 cm^{-1} has been well identified as the "free OH" stretch mode for the water OH bond whose H terminal is not hydrogen-bonded to a neighboring molecule. The other two peaks can be identified as the "bonded OH" stretch modes. The one at lower frequency corresponds to an ordered structure in which the two H terminals of the water molecule are hydrogen-bonded evenly to the neighboring molecules as in the case of ice. The one at higher frequency corresponds to a disordered structure in which the two H terminals of the water molecule are bonded unevenly to the neighboring molecules. This assignment is supported by the ice vibrational spectrum peaking sharply at 3200 cm^{-1}, as shown in Fig 4(D). Figure 4(B) yields directly two important pieces of information: First, the observed spectrum must be a vibrational spectrum of the surface water monolayer because otherwise the free OH peak cannot be present considering that water molecules beneath the surface must be fully hydrogen-bonded to the neighboring molecules. Second, the free OH peak

indicates that some surface water molecules must have at least one of their H terminals pointing out of the liquid. It was found that the free OH peak can be completely suppressed by imposing 0.25 monolayer of methanol or alcohol on the water surface. Knowing that each methanol molecule would connect with one dangling OH bond, we are then led to the conclusion that on the free water surface, 25% of the water molecules should have one of their H terminals pointing out of the liquid. This result immediately suggests that the free water surface structure resembles that of the hexagonal surface of ice, although as a liquid, the structure is somewhat disordered as evidenced by the clear presence of the disordered peak in Fig. 4(B).

Figure 4(A) is the spectrum of water at the quartz/surfactant/water interface. It resembles that of Fig. 4(B) except that the bonded OH region looks more like that of ice. We note that this is a hydrophobic interface. Supposedly, hydrophobicity at the molecular level means little or no interaction between water molecules and the substrate. We now understand that the persistent presence of the dangling OH bonds at the interface is a signature of the hydrophobicity. In the case of Fig. 4(B), the water surface is essentially against a solid wall and therefore is no longer flexible. As a result, one would expect more ordering in its ice-like structure, as indeed manifested by the ice-like spectrum in the bonded OH region.

The oil/water interface is unquestionably hydrophobic. From what we have already learned, it should be possible to predict the OH vibrational spectrum for such an interface. First, there should be the presence of the free OH peak at 3700 cm^{-1}, which is the signature of hydrophobicity. Second, because the interface is flexible, we expect the spectrum in the bonded OH region to resemble that of the air/water interface. As shown in Fig.4(C) for the hexane/water interface, this is indeed the case. The present example is a good illustration of how SFG can yield valuable surface spectroscopic information not attainable by other means and contribute to the advance of fundamental science.

In conclusion, the message we would like to convey here is that while the development of organic materials for nonlinear optics could be important for future optoelectronic applications, it is also interesting and profitable to use nonlinear optics as tools to study organic materials. A few more examples of the latter can be found in this special issue.

This work was supported by the Director, Office of Energy Research, Office of Basic Energy Sciences, Materials Science Division of the U.S. Department of Energy, under Contract No. DE-AC03-76SF00098, and by the National Science Foundation under Grant DMR-9025106.

References

1. See, for example, Y. R. Shen, *The Principles of Nonlinear Optics* (J. Wiley, New York, 1984).
2. W. Kraetschmer, L. D. Lamb, K. Fostiropoulos, and D. R. Huffman, *Nature* **347**, 354 (1990).
3. See, for example, H. Hoshi et al, *Jap. J. Appl. Phys. Lett.* (Part 2) **30**, L1397 (1991); X. K. Wang et al., *Appl. Phys. Lett.* **60**, 810 (1992); W. J. Blau et al, *Phys. Rev. Lett.* **67**, 1423 (1991); Z. H. Kafafi et al., *Chem. Phys. Lett.* **188**, 492 (1992); J. S. Meth et al., *Chem. Phys. Lett.* **197**, 26 (1992).
4. B. Koopmans, A. M. Janner, H. T. Jonkman, G. A. Sawatzky, and F. van der Wonde, *Phys. Rev. Lett.* **71**, 3569 (1993); B. Koopmans, A. Anema, H. T. Jonkman, G. A. Sawatzky, and F. van der Wonde, *Phys. Rev. B* **48**, 2759 (1993).
5. D. Wilk, D. Johannsmann, C. Stanners and Y. R. Shen, (to be published).
6. See, for example, B. Jerome, *Rep. Prog. Phys.* **54**, 391 (1991).
7. M. B. Feller, W. Chen, and Y. R. Shen, *Phys. Rev. A* **43**, 6778 (1991); Y. R. Shen, *Liquid Crystals* **5**, 635 (1989); D. Johennsmann, H. Zhou, P. Sounderkaer, H. Wierenga, B. O. Myrvold, and Y. R. Shen, *Phys. Rev. E* **48**, 1889 (1993); X. Zhuang, L. Marrucci, and Y. R. Shen (to be published).
8. J. M. Geary, J. W. Goodby, A. R. Kinetz, and J. S. Patel, *J. Appl. Phys.* **62**, 4100 (1987).
9. Q. Du, R. Superfine, E. Freysz and Y. R. Shen, *Phys. Rev. Lett.* **70**, 2313 (1993); Q. Du, E. Freysz and Y. R. Shen, *Phys. Rev. Lett.* **72**, 238 (1994); Q. Du, E. Freysz and Y. R. Shen, *Science* **264**, 826 (1994).

Figure Captions

Fig. 1 SHG versus film thickness from a C_{60} film grown at room temperature. The lines are the theoretical fit to the experimental data (circles) using the 7 parameter model.
(a) fundamental input s-polarized and reflected SH output p-polarized;
(b) fundamental input s-polarized and transmitted Sh output p-polarized;
(c) fundamental input p-polarized and reflected SH output p-polarized (open circles) fundamental input p-polarized and transmitted SH output p-polarized (solid circles)
(d) fundamental input mixed-polarized and reflected SH output s-polarized;
(e) fundamental input mixed-polarized and transmitted SH output s-polarized
(f) fundamental input mixed-polarized and reflected SH output p-polarized;
(g) fundamental input mixed-polarized and transmitted SH output p-polarized.

Fig 2 Output second-harmonic field (arbitrary units) vs sample rotation from 8 CB monolayers on a polyimide-coated substrate. Open squares are data from unrubbed substrates, filled circles are data from rubbed substrates, and solid lines are the theoretical fits. The input-output polarization combinations are (a) *p*-in/*p*-out; (b) *s*-in/*p*-out; (c) *s*-in/*s*-out; (d) *p*-in/*p*-out. Inset: Coordinates (x,y,z) used in the analysis in relation to the fixed laboratory coordinates (X,Y,Z = z). The plane of incidence is X-Z.

Fig. 3 Azimuthal orientational distribution functions of an.8CB monolayer on a rubbed polyimide-coated substrate (solid line), and an 8CB interfacial layer between a rubbed polyimide-coated surface and an 8CB bulk (dashed line)

Fig. 4 SFG spectra from (A) the quartz/OTS/water interface; (B) the air/water interface; (C) the hexane/water interface; and (D) the quartz/ice interface. The SF output, visible input IR input are s-, s-, and p-polarized, respectively.

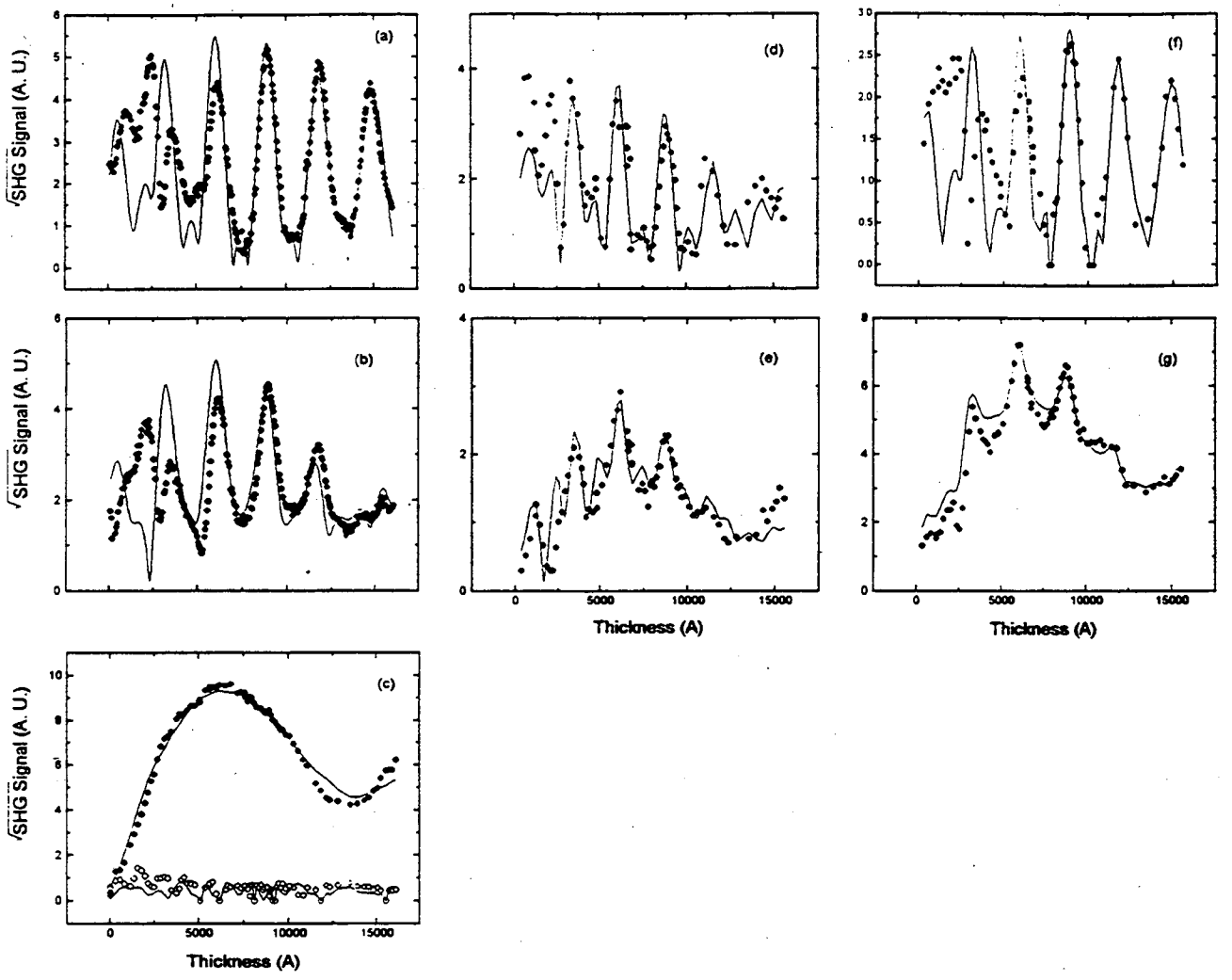

SHEN, Y. R.
Fig. 1 (a),(b),(c),(d),
(e),(f),(g)

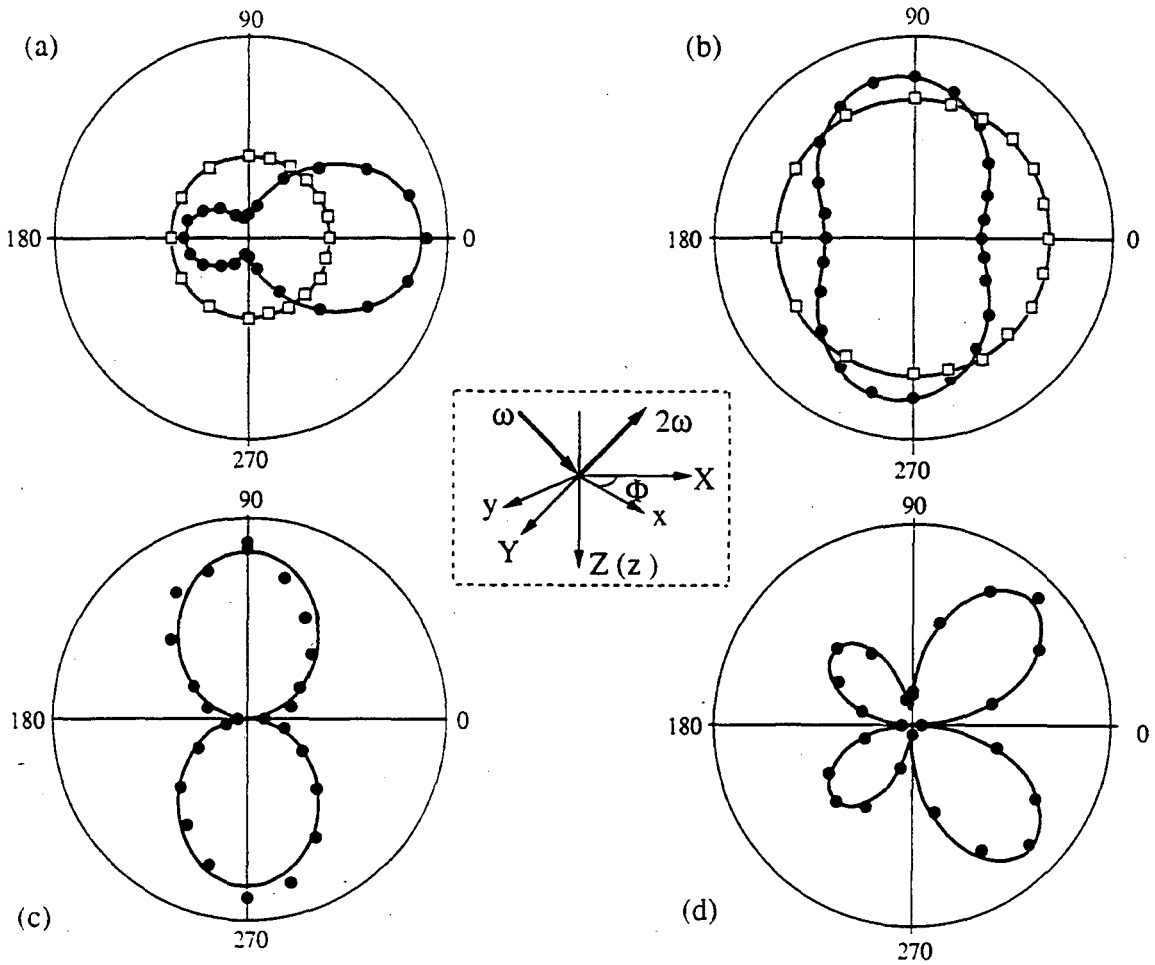

SHEN, Y. R.
Fig. 2 (a),(b),(c),(d)

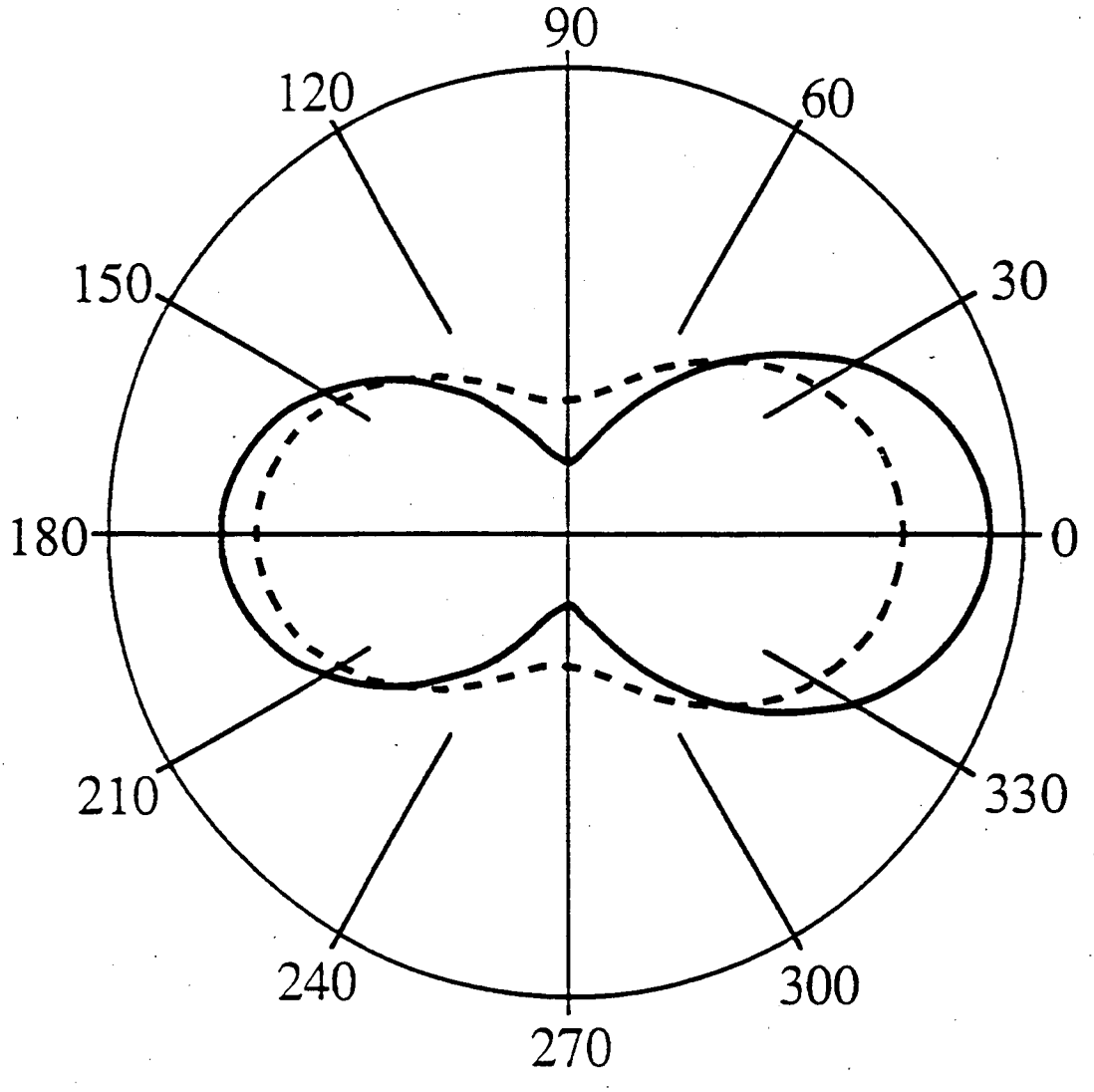

SHEN, Y. R.
Fig. 3

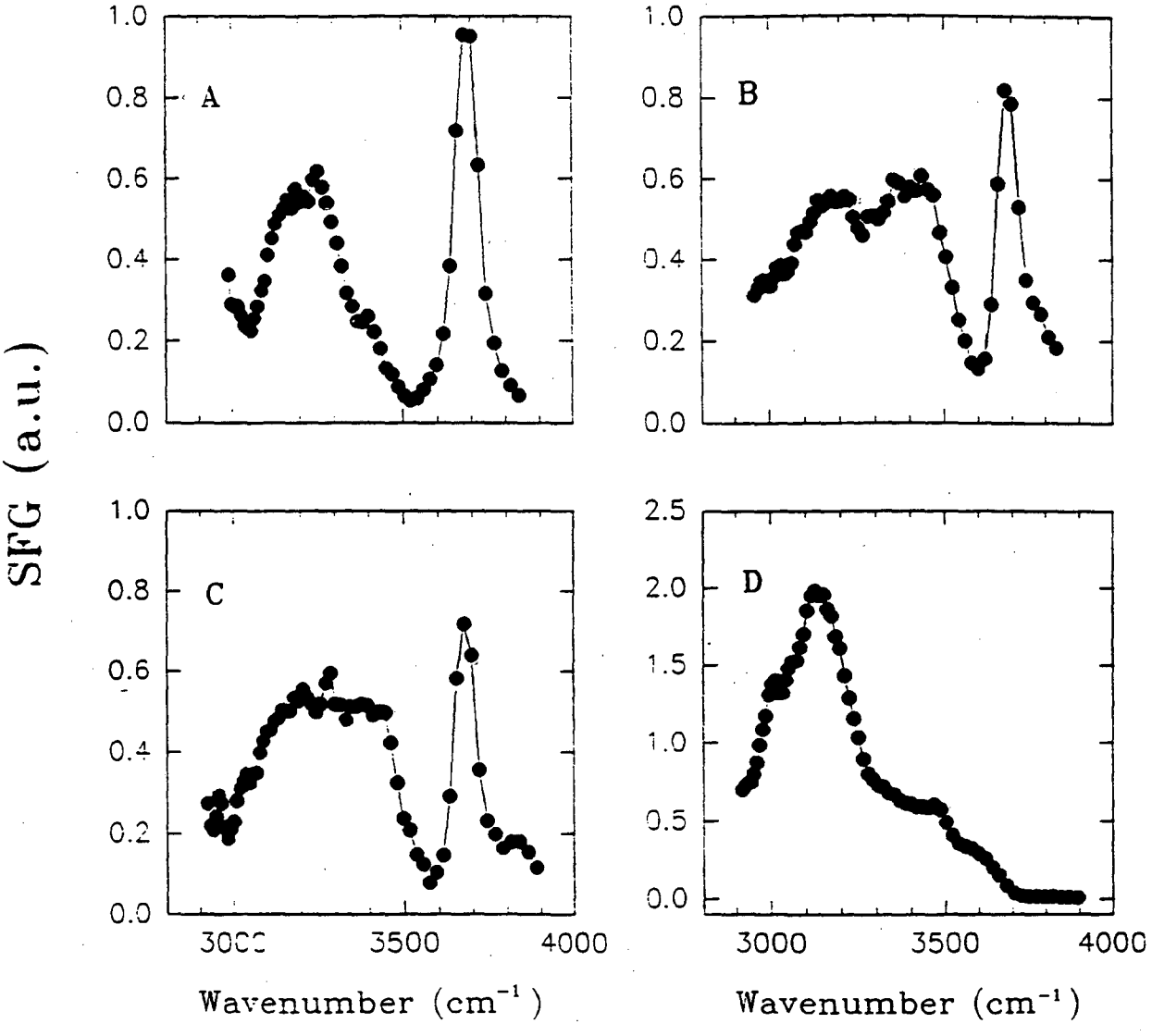

SHEN, Y. R.
Fig. 4 (a),(b),(c),(d)

LAWRENCE BERKELEY LABORATORY
UNIVERSITY OF CALIFORNIA
TECHNICAL INFORMATION DEPARTMENT
BERKELEY, CALIFORNIA 94720